AGU PUBLICATIONS

Geophysical Research Letters

RESEARCH LETTER
10.1002/2016GL068539

Key Points:
- Algorithms are developed for estimation of pH from biogeochemical floats in the Southern Ocean
- The pH algorithms can also be used to adjust pH sensor data on biogeochemical floats
- The seasonal cycle in surface pH ranges from 0.05 to 0.08 for the study region

Supporting Information:
- Supporting Information S1

Correspondence to:
N. L. Williams,
nancy.williams@oregonstate.edu

Citation:
Williams, N. L., L. W. Juranek, K. S. Johnson, R. A. Feely, S. C. Riser, L. D. Talley, J. L. Russell, J. L. Sarmiento, and R. Wanninkhof (2016), Empirical algorithms to estimate water column pH in the Southern Ocean, *Geophys. Res. Lett.*, *43*, 3415–3422, doi:10.1002/2016GL068539.

Received 4 MAR 2016
Accepted 22 MAR 2016
Accepted article online 28 MAR 2016
Published online 7 APR 2016

Empirical algorithms to estimate water column pH in the Southern Ocean

N. L. Williams[1], L. W. Juranek[1], K. S. Johnson[2], R. A. Feely[3], S. C. Riser[4], L. D. Talley[5], J. L. Russell[6], J. L. Sarmiento[7], and R. Wanninkhof[8]

[1]College of Earth, Ocean, and Atmospheric Sciences, Oregon State University, Corvallis, Oregon, USA, [2]Monterey Bay Aquarium Research Institute, Moss Landing, California, USA, [3]Pacific Marine Environmental Laboratory, National Oceanic and Atmospheric Administration, Seattle, Washington, USA, [4]School of Oceanography, University of Washington, Seattle, Washington, USA, [5]Scripps Institution of Oceanography, University of California, San Diego, La Jolla, California, USA, [6]Department of Geosciences, University of Arizona, Tucson, Arizona, USA, [7]Program in Atmospheric and Oceanic Sciences, Princeton University, Princeton, New Jersey, USA, [8]Atlantic Oceanographic and Meteorological Laboratory, National Oceanic and Atmospheric Administration, Miami, Florida, USA

Abstract Empirical algorithms are developed using high-quality GO-SHIP hydrographic measurements of commonly measured parameters (temperature, salinity, pressure, nitrate, and oxygen) that estimate pH in the Pacific sector of the Southern Ocean. The coefficients of determination, R^2, are 0.98 for pH from nitrate (pH^N) and 0.97 for pH from oxygen (pH^{Ox}) with RMS errors of 0.010 and 0.008, respectively. These algorithms are applied to Southern Ocean Carbon and Climate Observations and Modeling (SOCCOM) biogeochemical profiling floats, which include novel sensors (pH, nitrate, oxygen, fluorescence, and backscatter). These algorithms are used to estimate pH on floats with no pH sensors and to validate and adjust pH sensor data from floats with pH sensors. The adjusted float data provide, for the first time, seasonal cycles in surface pH on weekly resolution that range from 0.05 to 0.08 on weekly resolution for the Pacific sector of the Southern Ocean.

1. Background

As atmospheric carbon dioxide (CO_2) continues to increase due to fossil fuel burning, cement production, and land use changes [*Tans*, 2009; *Rhein et al.*, 2013], only ~42 ± 4% of this excess carbon stays in the atmosphere, while the remaining ~58 ± 15% is absorbed by the ocean and by the terrestrial biosphere [*Le Quéré et al.*, 2015]. Observations and models indicate that the ocean has sequestered approximately 28% of all anthropogenic CO_2 released since the beginning of the industrial era [*Le Quéré et al.*, 2015], which has caused a corresponding decrease in surface ocean pH of approximately 0.1 [*Orr et al.*, 2005; *Dore et al.*, 2009]. Consequently, there is much demand for high-quality ocean carbon and pH data to elucidate the spatial and temporal patterns of CO_2 uptake and show how these are changing ocean chemistry and ecosystems.

The Southern Ocean plays a major role in the uptake, transport, and long-term storage of heat and CO_2 accounting for over 40% of the total ocean carbon sink [*Khatiwala et al.*, 2009; *Frölicher et al.*, 2015]; yet it remains one of the least-sampled regions of the ocean. The Southern Ocean Carbon and Climate Observations and Modeling (SOCCOM, http://soccom.princeton.edu) project is shedding light on this important region by deploying approximately 200 profiling floats with novel biogeochemical sensors over five years. Following Argo protocols, each SOCCOM biogeochemical float executes a profile between the surface and ~2000 m (dependent upon ballasting) every 10 days and is equipped with temperature (T), salinity (S), and pressure (P) sensors as well as at least two of the four following biogeochemical sensors: Deep-Sea DuraFET pH [*Martz et al.*, 2010; *Johnson et al.*, 2016], ISUS or SUNA nitrate [*Johnson et al.*, 2013], oxygen optode [*Körtzinger et al.*, 2005], and WET Labs ECO FLbb-AP2 fluorescence and backscatter [*WET Labs*, 2009] (additional sensor information is provided in Table S1 in the supporting information). A calibration CTD (conductivity, temperature, depth) cast with discrete bottle measurements is performed right after each SOCCOM biogeochemical float deployment, and data from these casts are used to correct for any initial sensor offsets.

As described in *Juranek et al.* [2009, 2011], measurements of oxygen (O_2) and/or nitrate (NO_3^-) can be used in conjunction with measurements of T, S, and P to accurately estimate pH and other carbonate system parameters, expanding the utility of these floats. This approach is based on the fact that changes in carbonate system parameters are governed by physics and biology and should therefore be a function of T, S, and either

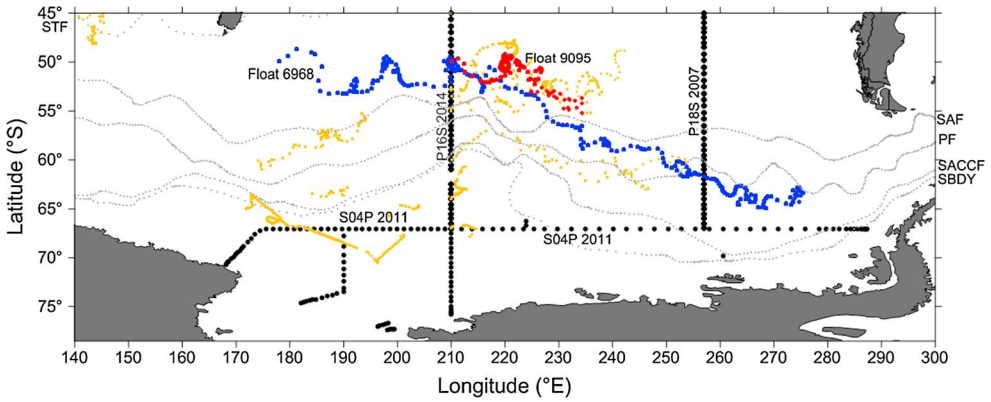

Figure 1. Map of the trajectories for all SOCCOM and pre-SOCCOM profiling floats in the Pacific sector (colored dots; generally moving eastward) with the two floats used for this study shown in blue (float 6968) and red (float 9095), the locations of the discrete bottle measurements (black dots), and the locations of the Antarctic Circumpolar Current (ACC) fronts (grey dotted lines) from *Orsi et al.* [1995]. From north to south the fronts are as follows: the Subtropical Front (STF), the Subantarctic Front (SAF), the Polar Front (PF), the Southern ACC Front (SACCF), and the Southern ACC Boundary (SBDY).

O_2 or NO_3^- and that the thermodynamic relationships between carbonate system parameters can be characterized by *T*, *S*, and *P* [*Lueker et al.*, 2000]. Others have proposed similar algorithms for pairs of carbonate system parameters that could be used to calculate pH for this region [*Bostock et al.*, 2013; *Velo et al.*, 2013; *Carter et al.*, 2016]; however, the algorithms presented here are the first to directly estimate pH and show much smaller errors by limiting their scope to the Southern Ocean. For floats without pH sensors, an algorithm for estimating pH shows the seasonal dynamics of the carbonate system along a float's trajectory and increases the spatial resolution of the pH data set. The pH algorithms are also critical for evaluating float pH sensor performance and adjusting for offsets and drift. The utility of these algorithms is not limited to floats but can be expanded to estimate pH using shipboard measurements or using data from other autonomous platforms such as gliders or moorings that measure *T*, *S*, *P*, NO_3^-, or O_2, or applied to climate model simulations. Accurate pH, when combined with estimates of alkalinity, can be used to calculate other carbonate system parameters such as dissolved inorganic carbon (DIC), the partial pressure of carbon dioxide (pCO_2), and the saturation state of aragonite (Ω_{Ar}) and calcite (Ω_{Ca}).

2. Development of pH Algorithms

We used the method described in *Juranek et al.* [2009, 2011] to develop two multiple linear regression (MLR) algorithms for pH for the Pacific sector of the Southern Ocean south of 45°S. To develop these algorithms, high-quality discrete bottle measurements were used that were collected on GO-SHIP repeat hydrographic cruises S04P 2011 (67°S) and P16S 2014 (150°W) (Figure 1, black dots). Only direct spectrophotometric measurements of pH are utilized to train the algorithms as compared to pH calculated from other measured carbonate system parameters in previous studies of this kind [*Juranek et al.*, 2011; *Alin et al.*, 2012]. The reported uncertainties in the pH measurements used in this study are 0.003 (S04P 2011) and 0.0013 (P16S 2014), whereas the uncertainty in pH calculated using measurements of dissolved inorganic carbon (DIC) and total alkalinity with uncertainties of ±2 and ±3 μmol kg^{-1}, respectively, is 0.01. Both of these methods have an additional uncertainty of up to 0.01 when converting from lab pressure to in situ pressure and from measurement temperature of pH of 20 or 25°C to in situ temperatures at 2000 dbar due to uncertainties in the pressure and temperature coefficients for carbonate system calculations. These MLR algorithms capture changes in pH due to biological activity but do not account for changes in anthropogenic CO_2 because such changes are not accompanied by a change in oxygen or nitrate. Discrete spectrophotometric pH data are also available for P18S 2007 [*Feely et al.*, 2008]; however, we did not use this data set for pH algorithm development due to offsets in pH in the deep water possibly due to impurities in the indicator dye used to measure pH of the P18S 2007 cruise and differences in the anthropogenic CO_2 concentrations in the upper water column and therefore differences in pH for this earlier cruise. Relative to the P16S 2014 and S04P 2011 data sets, the

P18S 2007 data set is higher by 0.012 in water masses that were recently in contact with the atmosphere, which is consistent with the observed anthropogenic ocean acidification of 0.002 year^{-1} in this region [*Williams et al.*, 2015]. Because anthropogenic pH changes between 2007 and 2015 did not influence pH at levels around 1500 m, we used the deep discrete bottle data from P18S 2007 to evaluate algorithm performance in the eastern portion of the basin (supporting information Figure S1). All pH data are reported at in situ pressures and temperatures on the total scale (pH_{Total}). The CO2SYS MATLAB program [*Lewis and Wallace*, 1998; *van Heuven et al.*, 2011] and the constants of *Lueker et al.* [2000], *Dickson* [1990], and *Perez and Fraga* [1987] were used for all carbonate system calculations.

The algorithms were created using parameters that are measured on the SOCCOM biogeochemical floats: *T*, *S*, *P*, O_2, and NO_3^-. Discrete bottle data south of 45°S and shallower than 2100 m were used, but data shallower than 100 m (average depth of the summer mixed layer) were excluded from any fits using O_2 as a predictor variable because of the decoupling of carbon and oxygen in the mixed layer (see section 3). We added predictor variables to the fits through forward stepwise regression while monitoring the coefficient of determination, R^2, and root-mean-square (RMS) error and checking for collinearity at each step by confirming that the variance inflation factor for each variable is less than 5 [*Kutner et al.*, 2004]. Because NO_3^- and O_2 provide similar information, none of the algorithms included both nitrate and oxygen as predictor variables. While NO_3^- and O_2 are comparable predictor variables for pH in this region (refer to supporting information Table S2 for R^2 and RMS errors), each has its strengths and weaknesses (see section 3). Two pH algorithms were created, each including *T*, *S*, and *P* and either O_2 (pH^{Ox}) or NO_3^- (pH^N) as a fourth predictor variable. We experimented with developing separate algorithms for each of the water masses between Antarctic Circumpolar Current (ACC) fronts or based on density layers, but these algorithms did not exhibit significantly improved fit statistics, and the need to switch algorithm based on location decreased their utility. Including derived quantities such as density or apparent oxygen utilization as predictor variables did not improve the fits.

3. Results and Discussion

The pH^N and pH^{Ox} algorithms take the following forms:

$$pH^N = \beta_0 + \beta_1 S + \beta_2 T + \beta_3 P + \beta_4 N \quad (1)$$

$$pH^{Ox} = \beta_0 + \beta_1 S + \beta_2 T + \beta_3 P + \beta_4 O_2 \quad (2)$$

The R^2 values for pH^N and pH^{Ox} are 0.98 and 0.97, and the RMS errors are 0.010 and 0.008, respectively (see supporting information Table S2 for a summary of algorithm coefficients and statistics.) For the pH^N algorithm (surface to 2100 m), salinity explains 69% of the variability in pH, and for the pH^{Ox} algorithm (100 m to 2100 m), oxygen explains 74% of the variability in pH (determined by the R^2 for an algorithm trained using one single variable); however, the addition of subsequent predictor variables (*T*, *S*, and *P*) decreases the RMS errors and reduces biases in the spatial distribution of the fit residuals for both algorithms. Of note is that the seasonal cycle we observe in surface pH in this region is on the order of 0.05 to 0.08, which is more than 5 times larger than the RMS errors of the algorithms. While the algorithms presented here are optimized for the Pacific sector of the Southern Ocean, these algorithms perform well in the other sectors of the Southern Ocean (supporting information Figure S2).

As of 5 February 2016 there are a total of 33 operational SOCCOM floats (see float status table at http://soccom.princeton.edu/float_stats.php and Figure 1). We used the data from SOCCOM float 9095 (WMO ID 5904188) and pre-SOCCOM float 6968 (WMO ID 5903718) for this analysis. When the pH^N and pH^{Ox} algorithms were applied to SOCCOM float 9095, which has the full suite of biogeochemical sensors, we were able to evaluate the performance of the Deep-Sea DuraFET pH sensor and examine differences between the pH algorithms.

By comparing the difference between the sensor-measured pH and the algorithm-predicted pH^{Ox} and pH^N at 1500 m (Figure 2d), a downward drift was observed in measured pH relative to both algorithms over the first several months of deployment before measured pH leveled off at a stable mean offset of approximately −0.02. This offset is the result of a shift in the reference potential (equivalent to the standard potential of an electrochemical cell) of the Deep-Sea DuraFET reference sensor during the first several weeks of exposure to seawater [*Bresnahan et al.*, 2014; *Johnson et al.*, 2016]. This drift, which results from insufficient equilibration

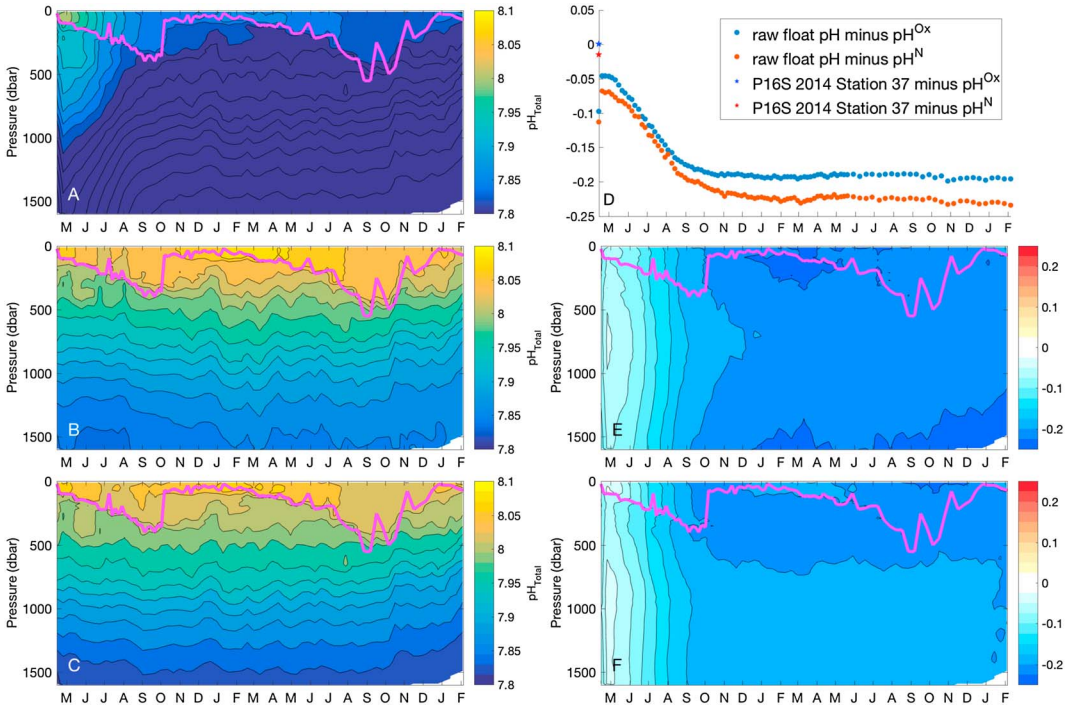

Figure 2. (a) Measured pH, (b) algorithm pH^N, and (c) algorithm pH^{Ox} plotted versus time for float 9095 with 0.02 contours. (d) Measured pH minus pH^N (red dots), measured pH minus pH^{Ox} (blue dots), and measured pH for the deployment cast P16S 2014 bottle data minus pH^N and pH^{Ox} (red and blue stars, respectively) all at 1500 m, plotted versus time, illustrating the drift in the pH and nitrate sensors over time. (e) Depth versus time contour plots of raw measured pH minus pH^N and (f) raw measured pH minus pH^{Ox} (bottom) for float 9095, both with 0.025 contours. The magenta line is the mixed layer depth [*Dong et al.,* 2008]. Float 9095 was deployed in April 2014 during the P16S GO-SHIP cruise [*Talley et al.*, 2014].

of the AgCl reference sensor with seawater bromide, is being addressed for future SOCCOM float deployments by more extensive exposure of the sensors to seawater before deployment. These differences between measured and algorithm-predicted pH through time between 1400 and 1600 m are being used to adjust pH sensor data from all SOCCOM floats and have become integral to the quality control process (see supporting information Text S1 for details). Note that the pH sensor on float 9095 has experienced more instrumental drift since deployment than any other SOCCOM float.

Because the sensor data used to calculate pH^N and pH^{Ox} in Figure 2 are corrected for initial offsets from the deployment calibration cast but are not corrected for any possible drift, we can use the difference between the sensor offset from pH^N and the sensor offset from pH^{Ox} at 1500 m (difference between the red and blue lines in Figure 2d) to examine for possible drift in the nitrate or oxygen sensors if we assume that the float temperature, salinity, and pressure sensors are stable through time. The decrease in $pH_{meas} - pH^N$ (red dots, Figure 2d) over time for float 9095 suggests that the ISUS nitrate sensor is drifting downward, which has been observed on other profiling floats [*Johnson et al.*, 2013]. *Johnson et al.* [2013] observed an average downward drift of 1 to 2 $\mu mol\,L^{-1}\,yr^{-1}$ in nitrate measured using ISUS sensors on several APEX profiling floats in the North Pacific, and this drift results in an overestimate in pH^N of 0.02 $year^{-1}$, which is on the order of what we calculate for float 9095. To correct for this drift in the nitrate sensor, we can apply an MLR algorithm for nitrate specific to this region (see supporting information Text S1 for details).

After the data have been adjusted for initial offsets and drift [*Johnson et al.*, 2016] (see supporting information Text S1 for details), we can compare the adjusted pH sensor data with the algorithm estimates for float 9095 (Figures 3a and 3b) to evaluate differences in the pH^N and pH^{Ox} algorithms. As the adjustment process involves only data at 1500 m, the annual cycle observed with the sensors at the surface is unaffected by the adjustment. In the surface mixed layer, the pH^N algorithm generally outperforms pH^{Ox}. Because the timescale for CO_2 exchange with the atmosphere (months) is much slower than that for oxygen (weeks), the O_2:C

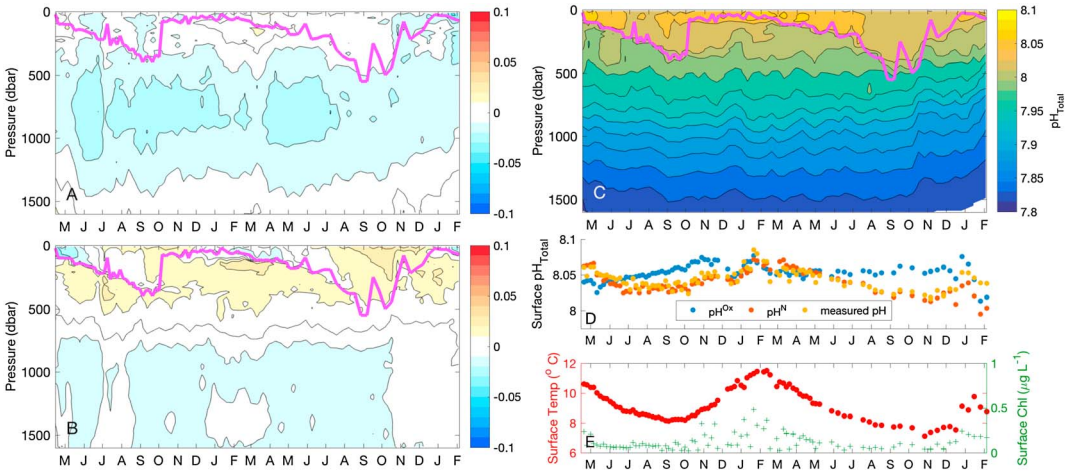

Figure 3. (a) Algorithm-predicted pH^N minus adjusted float-measured pH and (b) algorithm-predicted pH^{Ox} minus adjusted float-measured pH with 0.01 contours for SOCCOM float 9095. The magenta line is the mixed layer depth [*Dong et al.,* 2008]. (c) Adjusted float-measured pH with 0.02 contours. (d) Surface pH^{Ox} (blue), surface pH^N (red), and adjusted float-measured surface pH (yellow) for SOCCOM float 9095. (e) Float-measured sea surface temperature (red dots) and chlorophyll (green crosses, calculated using factors based on a comparison of sensor values and discrete chlorophyll samples when the float was launched (E. Boss and N. Haentjens, personal communication, 2016)) for float 9095. Float 9095 was deployed in April 2014 during the P16S GO-SHIP cruise [*Talley et al.*, 2014].

stoichiometry decouples during times of intense surface oxygen supersaturation or undersaturation. In summer, oxygen supersaturation leads to outgassing of oxygen and causes the pH^{Ox} algorithm to underestimate surface pH. In late winter, when respiration dominates leading to surface oxygen undersaturation and ingassing of oxygen, the pH^{Ox} algorithm overestimates surface pH. The pH^{Ox} algorithm also has increased errors in areas of active deep water formation, where oxygen and carbon may not have sufficient time to come to equilibrium with the atmosphere before the water mass is subducted [*Jacobs*, 2004]. Thus, pH^N is preferable over pH^{Ox} for estimating pH near the surface and should be used when high-quality nitrate data are available; however, the pH^N algorithm does exhibit increased prediction error in surface waters between the Subantarctic Front (SAF) and the Polar Front (PF) in the main jet of the ACC due to the significant water mass mixing and transformation occurring at these fronts and limited training data from this dynamic region. After the nitrate sensor is adjusted for drift (see supporting information Text S1), the pH^{Ox} and pH^N algorithms perform equally well below the depth of the winter mixed layer (≈500 m).

Float 9095, which remained north of the main jet of the ACC throughout the study period, has a seasonal cycle in surface pH of approximately 0.08 (Figure 3d). This is similar in magnitude to the surface seasonal cycle observed at Southern Ocean Time Series [*Shadwick et al.*, 2015], which is just south of Tasmania and is also located between the Subtropical Front (STF) and SAF, and at Bermuda Atlantic Time Series [*Bates et al.*, 2012] in the northern Atlantic subtropical gyre. It is larger, however, than the 0.03 to 0.04 surface seasonal cycle observed at Station ALOHA in the North Pacific subtropical gyre [*Dore et al.*, 2009], at European Station for Time series in the Ocean Canary Islands in the northeastern subtropical Atlantic [*Santana-Casiano et al.*, 2007; *González-Dávila et al.*, 2010], and at Station P (Ocean Station Papa) in the subarctic Pacific [*Emerson et al.*, 2011]. The surface pH on float 9095 (Figure 3) is lowest in the winter months when primary production is low and the deep winter mixed layer entrains older, more CO_2-enriched waters from below. In the spring, when the mixed layer shallows, primary production removes CO_2, increasing surface pH through summer and dominating over the decrease in pH that would be expected from seasonal warming. As the mixed layer deepens in fall, this high pH surface signal is mixed away and the surface pH drops. The float 9095 surface record (Figure 3d) shows that the pH^N algorithm better estimates the seasonal cycle in surface pH than the pH^{Ox} algorithm, due to the differences described in the previous paragraph.

We then applied the pH^N algorithm to pre-SOCCOM biogeochemical Argo float 6968, which was deployed in March 2012 at 50°S south of New Zealand and does not have a pH sensor but has over three years crossed multiple fronts. Estimated pH^N along the trajectory for float 6968 (Figure 4a) shows the general decreasing

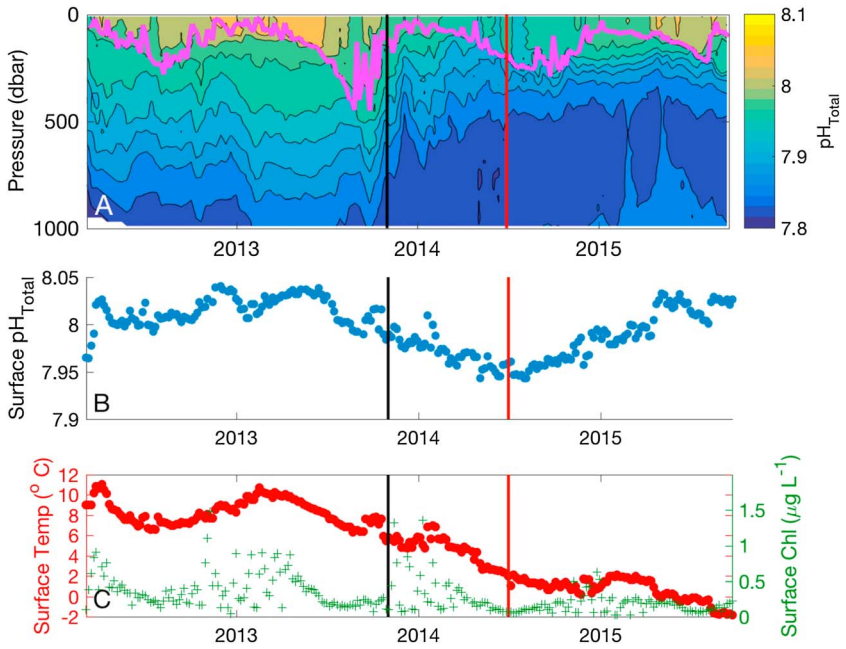

Figure 4. (a) Estimated pH^N for pre-SOCCOM float 6968 (deployed just south of New Zealand) with 0.025 contours. The magenta line is the mixed layer [*Dong et al.,* 2008], the thick black and red vertical lines are the times at which the float crossed the Subantarctic Front (northern boundary of the ACC characterized by geopotential height anomaly of 0.90 J/kg [*Orsi et al.*, 1995]) and the Polar Front (characterized by year-round surface water temperatures <2°C), respectively. (b) Estimated surface pH^N for pre-SOCCOM float 6968. (c) Float-measured sea surface temperature (red dots) and chlorophyll (green crosses, calculated using factory calibration) for float 6968.

trend in estimated pH from north to south across the ACC. As the float moves from the subtropics south across the SAF (Figure 4, vertical black line) into the ACC, pH at depth decreases as the predominance of circumpolar deep water (CDW) increases. In the ACC region the prevailing winds are westerly, which move surface water northward via Ekman transport, and old, carbon-rich CDW outcrops to replace it [*Speer et al.*, 2000]. The CDW has a relatively low estimated pH, because it has been isolated from the atmosphere for longer than any other water mass we observe on this float trajectory, and it has a large respiration signal. Discrete observations from P16S (150°W) and P18S (110°W) show that there is little east-west gradient in water mass characteristics south of 45°S in this region and that the crossing of the quasi-zonal ACC fronts dominates trends in float observations.

The estimated surface pH on float 6968 (Figure 4b) is mainly controlled by seasonality in primary productivity and mixed layer depth; however, the cross-frontal movement of the float convolutes this seasonal pattern. During most of 2012 and 2013 the float was located north of the main jet of the ACC in the subtropical Pacific, where in the summer, primary productivity removes CO_2 from the surface waters and drives pH upward, and in the winter, pH drops again as primary productivity slows, the mixed layer deepens, and respiration causes enrichment of CO_2 in the surface waters. As the float moves southward across the SAF and crosses into the ACC (Figure 4, black vertical line), the surface pH drops significantly due to the increased influence of the outcropping CDW. The seasonal cycle in surface pH within the ACC is muted relative to the subtropics due to the strong presence of upwelled CDW at the surface year round. As the float continues to move southward and crosses the Polar Front (Figure 4, red vertical line) where cold, fresh Antarctic Surface Water caps the surface of the water column and year-round surface water temperatures are less than 2°C (Figure 4C), surface pH is again mainly controlled by biological processes and mixed layer depth.

4. Summary

The algorithms presented here can be used to accurately estimate pH throughout the full seasonal cycle in the Pacific sector of the Southern Ocean where high-quality *T*, *S*, *P*, and oxygen or nitrate data are available and to adjust pH sensor data on biogeochemical floats. However, the algorithms do not account for the

observed anthropogenic ocean acidification of 0.002 year^{-1} in this region. Indeed, because the algorithms were trained using discrete data from between 2011 and 2014, they should not be used to estimate pH beyond approximately five years on either end of this time period, as this by itself would increase the bias in estimated pH due to increases in anthropogenic carbon inventories over that time. The algorithms do not account for changes in processes such as gas exchange that may modify the relationships between pH and the master variables used in the algorithm. With these caveats in mind, these algorithms can be a valuable asset toward understanding the seasonality in pH in this poorly observed region, and they may also be of use as initial conditions and validation in ocean carbon system models. The pH^N algorithm most accurately estimates pH in surface waters and is preferable over pH^{Ox} when high-quality nitrate data are available. The pH^{Ox} algorithm, however, has been most useful for SOCCOM float pH sensor adjustment because the pH^{Ox} algorithm performs well in deep waters and is not subject to issues with drift that the nitrate sensor currently experiences. These algorithms have been optimized using summer data for the Pacific sector in waters shallower than 2100 m, and further analysis is required to determine whether separate algorithms should be developed for each basin. Newly acquired high-quality discrete inorganic carbon data will be incorporated into updated algorithms in order to expand the seasonal and spatial range of the training data set, which will further expand the utility of these novel biogeochemical sensors.

Acknowledgments

The measurement methods, calibration, and quality control for all discrete bottle data used in this study are available at http://cchdo.ucsd.edu, and all SOCCOM float data are available at http://soccom.princeton.edu/soccomviz.php. This work was sponsored by the U.S. National Science Foundation's Southern Ocean Carbon and Climate Observations and Modeling (SOCCOM) Project under the NSF Award PLR-1425989. Logistical support for this project in Antarctic waters was provided by the U.S. National Science Foundation through the U.S. Antarctic Program. Additionally, we acknowledge support from U.S. Argo through NOAA/JISAO grant NA17RJ1232 to the University of Washington. Nancy Williams is also supported by the ARCS Foundation Portland Chapter. This is PMEL contribution 4417.

References

Alin, S. R., R. A. Feely, A. G. Dickson, J. M. Hernández-Ayón, L. W. Juranek, M. D. Ohman, and R. Goericke (2012), Robust empirical relationships for estimating the carbonate system in the southern California Current System and application to CalCOFI hydrographic cruise data (2005–2011), *J. Geophys. Res.*, *117*, C05033, doi:10.1029/2011JC007511.

Bates, N. R., M. H. P. Best, K. Neely, R. Garley, A. G. Dickson, and R. J. Johnson (2012), Detecting anthropogenic carbon dioxide uptake and ocean acidification in the North Atlantic Ocean, *Biogeosciences*, *9*(7), 2509–2522, doi:10.5194/bg-9-2509-2012.

Bostock, H. C., S. E. Mikaloff Fletcher, and M. J. M. Williams (2013), Estimating carbonate parameters from hydrographic data for the intermediate and deep waters of the Southern Hemisphere oceans, *Biogeosciences*, *10*(10), 6199–6213, doi:10.5194/bg-10-6199-2013.

Bresnahan, P. J., Jr., T. R. Martz, Y. Takeshita, K. S. Johnson, and M. LaShomb (2014), Best practices for autonomous measurement of seawater pH with the Honeywell Durafet, *Methods Oceanogr.*, *9*, 44–60, doi:10.1016/j.mio.2014.08.003.

Carter, B. R., N. L. Williams, A. R. Gray, and R. A. Feely (2016), Locally interpolated alkalinity regression for global alkalinity estimation, *Limnol. Oceanogr. Methods*, doi:10.1002/lom3.10087.

Dickson, A. G. (1990), Standard potential of the reaction: AgCl(s) + 1/2 H_2(g) = Ag(s) + HCl(aq), and the standard acidity constant of the ion HSO_4^- in synthetic sea water from 273.15 to 318.15 K, *J. Chem. Thermodyn.*, *22*(2), 113–127, doi:10.1016/0021-9614(90)90074-Z.

Dong, S., J. Sprintall, S. T. Gille, and L. Talley (2008), Southern Ocean mixed-layer depth from Argo float profiles, *J. Geophys. Res.*, *113*, C06013, doi:10.1029/2006JC004051.

Dore, J. E., R. Lukas, D. W. Sadler, M. J. Church, and D. M. Karl (2009), Physical and biogeochemical modulation of ocean acidification in the central North Pacific, *Proc. Natl. Acad. Sci. U.S.A.*, *106*(30), 12,235–12,240, doi:10.1073/pnas.0906044106.

Emerson, S., C. Sabine, M. F. Cronin, R. Feely, S. E. Cullison Gray, and M. Degrandpre (2011), Quantifying the flux of $CaCO_3$ and organic carbon from the surface ocean using in situ measurements of O_2, N_2, pCO_2, and pH, *Global Biogeochem. Cycles*, *25*, GB3008, doi:10.1029/2010GB003924.

Feely, R. A., C. L. Sabine, F. J. Millero, R. Wanninkhof, D. A. Hansell, J. L. Bullister, and G. C. Johnson (2008), Carbon dioxide, hydrographic, and chemical data obtained during the R/V *Ronald H. Brown* cruise in the Pacific Ocean on CLIVAR repeat hydrography section P18_2007 (Dec. 15, 2007–March 23, 2008), doi:10.3334/CDIAC/otg.CLIVAR_P18_2007.

Frölicher, T. L., J. L. Sarmiento, D. J. Paynter, J. P. Dunne, J. P. Krasting, and M. Winton (2015), Dominance of the Southern Ocean in anthropogenic carbon and heat uptake in CMIP5 models, *J. Clim.*, *28*(2), 862–886, doi:10.1175/JCLI-D-14-00117.1.

González-Dávila, M., J. M. Santana-Casiano, M. J. Rueda, and O. Llinás (2010), The water column distribution of carbonate system variables at the ESTOC site from 1995 to 2004, *Biogeosciences*, *7*(10), 3067–3081, doi:10.5194/bg-7-3067-2010.

Jacobs, S. S. (2004), Bottom water production and its links with the thermohaline circulation, *Antarct. Sci.*, *16*(4), 427–437, doi:10.1017/S095410200400224X.

Johnson, K. S., L. J. Coletti, H. W. Jannasch, C. M. Sakamoto, D. D. Swift, and S. C. Riser (2013), Long-term nitrate measurements in the ocean using the in situ ultraviolet spectrophotometer: Sensor integration into the APEX profiling float, *J. Atmos. Oceanic Technol.*, *30*(8), 1854–1866, doi:10.1175/JTECH-D-12-00221.1.

Johnson, K. S., H. W. Jannasch, L. J. Coletti, V. A. Elrod, T. R. Martz, Y. Takeshita, R. J. Carlson, and J. J. Connery (2016), Deep-Sea DuraFET: A pressure tolerant pH sensor designed for global sensor networks, *Anal. Chem.*, doi:10.1021/acs.analchem.5b04653.

Juranek, L. W., R. A. Feely, W. T. Peterson, S. R. Alin, B. Hales, K. Lee, C. L. Sabine, and J. Peterson (2009), A novel method for determination of aragonite saturation state on the continental shelf of central Oregon using multi-parameter relationships with hydrographic data, *Geophys. Res. Lett.*, *36*, L24601, doi:10.1029/2009GL040778.

Juranek, L. W., R. A. Feely, D. Gilbert, H. Freeland, and L. A. Miller (2011), Real-time estimation of pH and aragonite saturation state from Argo profiling floats: Prospects for an autonomous carbon observing strategy, *Geophys. Res. Lett.*, *38*, L17603, doi:10.1029/2011GL048580.

Khatiwala, S., F. Primeau, and T. Hall (2009), Reconstruction of the history of anthropogenic CO_2 concentrations in the ocean, *Nature*, *462*(7271), 346–349, doi:10.1038/nature08526.

Körtzinger, A., J. Schimanski, and U. Send (2005), High quality oxygen measurements from profiling floats: A promising new technique, *J. Atmos. Oceanic Technol.*, *22*(3), 302–308, doi:10.1175/JTECH1701.1.

Kutner, M. H., C. Nachtscheim, and J. Neter (2004), *Applied Linear Regression Models*, 4th ed., McGraw-Hill/Irwin, New York.

W. E. T. Labs (2009), WET Labs ECO FLbb-AP2 Fluorometer-Backscattering Meter, Datasheet FLbb-AP2 Rev. A. [Available at http://wetlabs.com/sites/default/files/documents/FLBB-datasheet-May2009_0.pdf.]

Le Quéré, C., et al. (2015), Global carbon budget 2014, *Earth Syst. Sci. Data*, *7*(1), 47–85, doi:10.5194/essd-7-47-2015.

Lewis, E., and D. W. R. Wallace (1998), Program developed for CO_2 system calculations, *ORNL/CDIAC-105*. [Available at http://cdiac.ornl.gov/oceans/co2rprt.html (Accessed 31 January 2014).]

Lueker, T. J., A. G. Dickson, and C. D. Keeling (2000), Ocean pCO_2 calculated from dissolved inorganic carbon, alkalinity, and equations for K_1 and K_2: Validation based on laboratory measurements of CO_2 in gas and seawater at equilibrium, *Mar. Chem.*, *70*(1–3), 105–119, doi:10.1016/S0304-4203(00)00022-0.

Martz, T. R., J. G. Connery, and K. S. Johnson (2010), Testing the Honeywell Durafet for seawater pH applications, *Limnol. Oceanogr. Methods*, *8*, 172–184, doi:10.4319/lom.2010.8.172.

Orr, J. C., et al. (2005), Anthropogenic ocean acidification over the twenty-first century and its impact on calcifying organisms, *Nature*, *437*(7059), 681–686, doi:10.1038/nature04095.

Orsi, A. H., T. I. Whitworth, and W. D. J. Nowlin (1995), On the meridional extent and fronts of the Antarctic Circumpolar Current, *Deep Sea Res., Part I*, *42*(5), 641–673, doi:10.1016/0967-0637(95)00021-W.

Perez, F. F., and F. Fraga (1987), Association constant of fluoride and hydrogen ions in seawater, *Mar. Chem.*, *21*(2), 161–168, doi:10.1016/0304-4203(87)90036-3.

Rhein, M., et al. (2013), Observations: Ocean, in *Climate Change 2013: The Physical Science Basis. Contribution of Working Group I to the Fifth Assessment Report of the Intergovernmental Panel on Climate Change*, edited by T. F. Stocker et al., pp. 255–315, Cambridge Univ. Press, Cambridge, U. K., and New York.

Santana-Casiano, J. M., M. González-Dávila, M.-J. Rueda, O. Llinás, and E.-F. González-Dávila (2007), The interannual variability of oceanic CO_2 parameters in the northeast Atlantic subtropical gyre at the ESTOC site, *Global Biogeochem. Cycles*, *21*, GB1015, doi:10.1029/2006GB002788.

Shadwick, E. H., T. W. Trull, B. Tilbrook, A. J. Sutton, E. Schulz, and C. L. Sabine (2015), Seasonality of biological and physical controls on surface ocean CO_2 from hourly observations at the Southern Ocean Time Series site south of Australia, *Global Biogeochem. Cycles*, *29*, 223–238, doi:10.1002/2014GB004906.

Speer, K., S. R. Rintoul, and B. Sloyan (2000), The diabatic deacon cell, *J. Phys. Oceanogr.*, *30*(12), 3212–3222, doi:10.1175/1520-0485(2000)030<3212:TDDC>2.0.CO;2.

Talley, L. D., K. Johnson, S. Riser, and T. C. Hennon (2014), SOCCOM biogeochemical profiling float deployments from GO-SHIP P16S (RVIB Nathaniel B. Palmer NBP1403), *SOCCOM Tech. Rep. 2014–1*. [Available at http://soccom.princeton.edu/sites/default/files/files/SOCCOM_2014?1_P16S_floats.pdf.]

Tans, P. (2009), An accounting of the observed increase in oceanic and atmospheric CO_2 and the outlook for the future, *Oceanography*, *22*(4), 26–35, doi:10.5670/oceanog.2009.94.

van Heuven, S., D. Pierrot, J. W. B. Rae, E. Lewis, and D. W. R. Wallace (2011), *MATLAB Program Developed for CO_2 System Calculations. ORNL/CDIAC-105b*, Carbon Dioxide Information Analysis Center, Oak Ridge National Laboratory, U.S. Department of Energy, Oak Ridge, Tenn.

Velo, A., F. F. Pérez, T. Tanhua, M. Gilcoto, A. F. Ríos, and R. M. Key (2013), Total alkalinity estimation using MLR and neural network techniques, *J. Mar. Syst.*, *111–112*, 11–18, doi:10.1016/j.jmarsys.2012.09.002.

Williams, N. L., R. A. Feely, C. L. Sabine, A. G. Dickson, J. H. Swift, L. D. Talley, and J. L. Russell (2015), Quantifying anthropogenic carbon inventory changes in the Pacific sector of the Southern Ocean, *Mar. Chem.*, *174*, 147–160, doi:10.1016/j.marchem.2015.06.015.